3D medical objects retrieval approach using SPHARMs descriptor and network flow as similarity measure

Leila C. C. Bergamasco*, Karla R. P. S. Lima†, Carlos E. Rochitte‡ and Fátima L. S. Nunes *†
* Electrical Engineering Department, Polytechnic School, University of São Paulo.
Av. Prof. Luciano Gualberto, travessa 3, 380 - 05508-010. São Paulo - Brazil
Email: leila.cristina@usp.br
†School of Arts, Sciences and Humanities, University of São Paulo.
Av. Arlindo Béttio, 1000 - 03828-000. São Paulo - Brazil
Emails: karla@ime.usp.br; fatima.nunes@usp.br
‡ Cardiology and Pulmonary Division of Heart Institute, Medical School, University of São Paulo.
Av. Dr. Eneas de Carvalho Aguiar, 44 - 05403-000. São Paulo - Brazil
Email: rochitte@incor.usp.br

***Abstract*—The data processing to obtain useful information is a trending topic in the computing knowledge domain since we have observed a high demand arising from society for efficient techniques to perform this activity. Spherical Harmonics (SPHARMs) have been widely used in the three-dimensional (3D) object processing domain. Harmonic coefficients generated by this mathematical theory are considered a robust source of information about 3D objects. In parallel, Ford-Fulkerson is a classical method in graph theory that solves network flows problems. In this work we demonstrate the potential of using SPHARMs along with the Ford-Fulkerson method, respectively as descriptor and similarity measure. This article also shows how we adapted the later to transform it into a similarity measure. Our approach has been validated by a 3D medical dataset composed by 3D left ventricle surfaces, some of them presenting Congestive Heart Failure (CHF). The results indicated an average precision of 90%. In addition, the execution time was 65% lower than a descriptor previously tested. With the results obtained we can conclude that our approach, mainly the Ford-Fulkerson adaptation proposed, has a great potential to retrieve 3D medical objects.**

I. Introduction

According to Stanford 2017 Medicine Health trends report [1], health care data is increasing annually by 48%. Nowadays we have an amount of 153 exabytes and it is expected a total data volume of 2,314 exabytes in 2020.

There is a growing interest of the society in collecting and processing these data in order to extract useful information to predict patients behavior, create preventive actions, and improve the medical assistance quality, for example. These actions could reduce the health care costs, a worldwide concern since the population is getting older [1].

Several techniques are being developed to support the health care data processing: Artificial Intelligence, Data Mining, Pattern Recognition and Information Retrieval play important roles in this scenario. Content-Based Image Retrieval (CBIR) technique has been largely used in medical applications to retrieve the most similar images from a database based on their content, but mainly focused on two-dimensional (2D) images [2]. The first researches involving application of CBIR concepts to three-dimensional (3D) medical objects are relatively recent and started in the last decade. Most of the approaches deals with primitive information of 3D objects such as volume, surface area, and mesh density. There is still a range of possibilities to be explored.

An underexplored alternative is related to Spherical Harmonics (SPHARMs), which discretizes 3D objects in one-dimensional frequencies. This discretization generates harmonic coefficients, which are unique values that can be used to differentiate 3D objects. SPHARMs are pointed out by several authors [3], [4] as a robust technique since it is capable of capturing very detailed information about the structure. This characteristic is useful for several diseases investigation problems such as Congestive Heart Failure (CHF), which causes subtle left ventricle deformations. To perform the CHF diagnosis, the physicians usually analyze at least 50 of Cardiac Magnetic Resonance Imaging (MRI) slices, which takes time and can cause fatigue [5]. Thus, computational techniques are necessary to support, as well as to contribute to faster and more precise diagnosis.

Besides the advantages above mentioned, SPHARMs have some particularities to be considered, mainly related to the amount of harmonic coefficients generated. Since the harmonic coefficients are directly proportional to the amount of vertices of the 3D object, the more vertices the 3D object has, the more coefficients will be created to describe it. To compare this quantitative information, it is possible to use similarity functions. In CBIR we note a predominance of L_p distances as similarity functions, which perform well for several problems [6]. However, other approaches such as graphs and Support Vector Machine (SVM) can be efficient alternatives to L_p distances, since they have flexibility to deal with different sizes

of feature vectors and they are sensitive to small differences present on 3D objects. [3].

Considering the background presented, this article proposes a novel approach to process and to retrieve 3D medical objects of left ventricle with CHF disease using: 1) SPHARMs as descriptor, and 2) an adaptation of Ford-Fulkerson algorithm to compute the residual flow of bipartite graphs to be used as similarity measure. We compared our approach with another approach previously developed using a shape-based descriptor named 3D Hough Transform and L_p distance as similarity function.

This article is organized as follows: Section II introduces three important concepts used in this paper: CBIR, SPHARMs and network flow in bipartite graphs respectively; Section III describes some related works that use SPHARMS to improve medical diagnosis; Section IV contains an overview of our approach; Section V details the methodology used; Section VI reports and discusses the results found, and Section VII reports the final remarks of this work.

II. Background

A. Content-Based Image Retrieval

3D CBIR retrieves from a database 3D objects similar to a 3D object given as a query. CBIR systems can be divided into following steps: preprocessing, feature extraction, and similarity comparison, which uses methods that are capable of measuring similarity among different objects.

In the preprocessing stage, algorithms are applied to enhance regions of interest or decrease noise. In 3D domain, we can, for example, use algorithms to improve the 3D object segmentation, reconstruction and/or reduce the 3D points cloud. In the features extraction step, quantitative information is extracted from different aspects of the 3D object such as shape, topological information, color, texture, statistics, among others. Finally, to compute the similarity among features vectors we can use distance functions, such as Euclidean or Manhattan distance, or other computational method such as graph matching, k-means, and machine learning [3], [7].

Regarding CBIR in 3D domain, there is a predominance of global descriptors, which consider the whole 3D object information. However, many times health care area has problems where the differences among 3D objects are subtle and has changes only in specific locals. For example, CHF causes small shape alterations on left ventricle mainly in the bottom of this cardiac structure. Thus, it is important to investigate how global descriptors can be adapted to be sensitive to noise or how new descriptors can be created to include local perspective.

B. Spherical Harmonics

SPHARMs are spherical functions that satisfy the Laplace's equation. These functions can be expressed as a linear combination of their harmonic coefficients (Equation 1). In Equation 1, the term a_{lm} is the complex harmonic coefficients matrix and $Y_l^m(\theta, \phi)$ are SPHARMs of degree l and order m for the spherical coordinates (θ, ϕ). Usually the m value respects the interval $[-l, l]$ and $l \in \mathbb{N}\ [0, \infty]$ [8].

$$f(\theta, \phi) = \sum_{l}^{\infty} \sum_{m=-l}^{l} a_{lm} Y_l^m(\theta, \phi) \tag{1}$$

SPHARMs computation can be divided into parts as shown in Figure 1. We can define each part as follows [9]:

1) Harmonics computation: the term $Y_l^m(\theta, \phi)$ in Equation 1 is the harmonic for a specific degree l, order m and spherical coordinates (θ, ϕ). The spherical coordinate θ represents the polar angle, and ϕ represents the azimuth. Computation of this term is showed in Equation 2, where N_l^m is the normalization factor, $P_l^m(cos\phi)$ is the Associate Legendre Polynomial and $e^{im\phi}$ is the complex exponential.

$$Y_l^m(\theta, \phi) = N_l^m P_l^m(cos\phi) e^{im\phi} \tag{2}$$

   a) Normalization factor is a binomial using the l and m values as input (Equation 3).

$$N_l^m = \sqrt{\frac{2l+1}{4\pi} \frac{(l-m)!}{(l+m)!}} \tag{3}$$

   b) Associated Legendre Polynomials are solutions for the general Legendre equation [10]. These polynomials can be expressed using an explicit sum, as shown in Equation 4, where l and m are the same variables previously in Equation 2, and k is a variable with initial value equals to zero, which depends on l and m values to determine its maximum value.

$$P(x)_l^m = (1-x^2)^{\frac{m}{2}} \sum_{k=0}^{\frac{l-m}{2}} \frac{(2l-2k!)}{2^l (l-k)! k! (l-2k-m)!} \omega \tag{4}$$

$$\omega = (-1)^k x^{(l-2k-m)} \tag{5}$$

   c) Complex exponential: according to Equation 6, this term is computed using Euler's identity, where i means the imaginary part of the complex number, ϕ is the azimuth angle, and m is the SPHARM order.

$$e^{im\phi} = cos(m\phi) + isin(m\phi) \tag{6}$$

2) Coefficients a_{lm}: are projections of $f(\theta, \phi)$ on each basis function $Y_l^m(\theta, \phi)$ over the sphere, as showed in Equation 7.

$$a_{lm} = \int_{\theta=0}^{\pi} \int_{\phi=0}^{2\pi} f(\theta, \phi) Y_l^m(\theta, \phi) sin(\theta) d\phi d\theta \tag{7}$$

After the computation of these steps, a vector of length N is obtained, where N is the number of vertices of the mesh that represents the 3D object. This vector is used as descriptor in our approach.

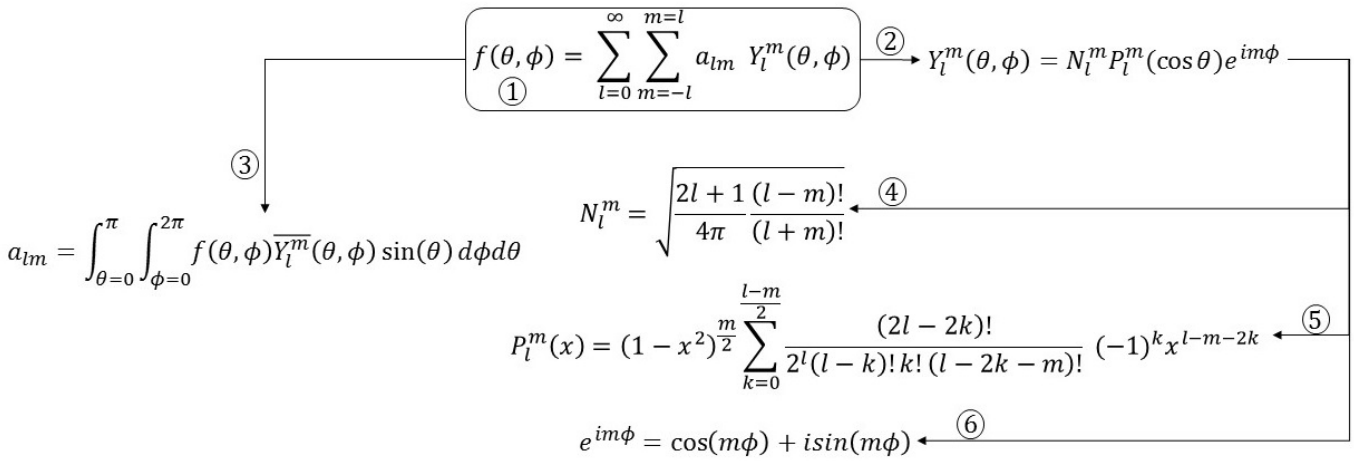

Figure 1. SPHARMs computation: (1) It is possible to separate the SPHARMs computation into two parts: the harmonics computation (2), composed by: Normalization factor (4), Associated Legendre polynomials (5) and complex exponential (6), and the second part is composed by the coefficient matrix computation (3).

C. Bipartite graphs and network flows

A graph G is a pair of (V, E), where V are vertices of G and E are the edges that connect different V, thus $E \subseteq [V^2]$. Two vertices x, y of G are called **adjacent** if they have an edge e connecting them. The edges are considered adjacent if they have a vertice v in common. If all the vertices of G are pairwise adjacent, the graph is denominated a **complete graph [11].**

A graph G is called *r-partite if G can be partitioned in r classes. In any r-partite graph*, two main requirements must be satisfied: 1) every edge has its termination in different classes, and 2) vertices of the same class cannot be adjacent. When the graph G is divided into two classes, it is called bipartite graph [11].

One of the bipartite graphs application is on network flows problems solution, such as optimization of electrical and telecommunication network and highways paths. Formally, a network flow $G = (V, E)$ is a digraph in which every edge has a non-negative **capacity** $c(u, v) \geq 0$. Two vertices are mandatory in this type of graph: the source s and the sink node t. All the graph nodes must be present in some part of the path from s to t [8].

D. Ford-Fulkerson algorithm

Several approaches can be used to solve network problems and the maximum flow is one of them. In this strategy, the goal is to identify which is the maximum capacity that each edge can withstand. Therefore, the network flow can transport the maximum of material from the source until the sink in an efficient path.

The Ford-Fulkerson algorithm is a classical approach to solve maximum flows problem. It consists in iteratively increasing the flow, determining an **augmenting path** [8]. Thus, the flow $f(v, u) = 0$ increases until the edges capacity reaches its limit. This process is done with the support of **residual flow**, which stores in memory the maximum capacity of each edge, and consequently starts the algorithm with value equal to the sum of all the edges capacities . Also iteratively as the method is executed, the residual flow decreases in the same proportion as the augmenting path grows. Equation 8 shows the relationship between an original flow f and their respective residual flow f' when the flow is augmented ($f \uparrow f'$).

$$(f \uparrow f') = \begin{cases} f(u,v) + f'(u,v) & \text{if } (u,v) \in E \\ 0 & \text{if } not \end{cases} \quad (8)$$

The algorithm uses Breadth-First Search to find the augmenting paths and Figure 2 shows a network flow with the used capacity (in red).

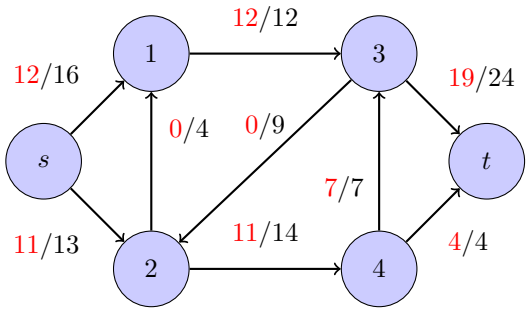

Figure 2. Example of a network flow with non-negative capacities in each edge.

Extending this concept to bipartite graphs we noted a specific behavior: when two classes have similar edges capacities, the residual flow value is small compared to edges having very different capacities. In this case, the residual flow is higher. Thus, this characteristic favors that the total residual flow value be used as a similarity measure.

III. Related Works

The SPHARMs utilization in 3D medical objects is relatively new, started in the last decade. The main goal of those

researches was to analyze and quantify 3D shapes or volumes.

In [12], SPHARMs were used to map the left ventricle and then compared them considering two different states (dilated and relaxed). In [13], SPHARMs was used to compare the volume and the shape of the amygdala–hippocampal between patients with and without schizophrenia. Authors state that the proposal was able to find a strong correlation between the shape of this structure and the schizophrenia presence.

Other papers such as [14]–[20] reported positive results in the quantification of 3D medical objects using SPHARMs. None of these cited papers used CBIR concepts to retrieve 3D objects, i.e., the authors did not use the quantitative information extracted as a feature vector in order to compare these vectors through similarity measure.

Even if not related to 3D medical objects retrieval, Kazhdan *et al.* [21] did an important improvement on SPHARMs, turning SPHARMs rotation invariant, a desirable characteristic for CBIR descriptors. They reached an average precision greater than 70% on their approach, which used Euclidean distance based on the SPHARMs coefficients sum. This work was used as basis for the SPHARMs implementation of this current work.

IV. Overview of the proposed approach

Taking advantage of specific characteristics of each technique (CBIR, SPHARMs and network flows we propose a novel approach that uses SPHARMs as descriptor, stores the data extracted in bipartite graphs and applies Ford-Fulkerson method as similarity measure. These techniques are detailed in the next subsections.

A. Descriptor and Storage

We applied SPHARMs algorithm to extract the quantitative information of the 3D left ventricles, and computed their harmonic coefficients. We implemented the algorithm following the Section II.B equations, providing the representation of the 3D object an one-dimensional n-length vector, where n is the amount of vertices of the 3D object. Then, we arranged the coefficients in each part of a bipartite graph to compare them. In Figure 3, c_i is the h_i^{th} harmonic coefficient h of the 3D medical object. Each set of coefficients is grouped in one side of the bipartite graph, represented in Figure 3 as Q (query) and C (consulted).

B. Ford-Fulkerson

To compute the similarity measure we used the total sum of residual flow generated by Ford-Fulkerson method. The main goal here is the harmonic coefficient utilization as edge capacity. After running the Ford-Fulkerson method, the residual flow is obtained and its sum is used as a dissimilarity value between two 3D medical objects.

To adequate this approach to our problem, several adaptations were made. Firstly, we noted that the SPHARMs generate negative values on their harmonic coefficients, and this behavior does not allow using them as edge capacity information. Thus, we performed a displacement in the harmonic coefficient values. In order to perform this, we found the most negative number between all the harmonic coefficients, computed the difference between it and the less non-negative number and summed this difference in all harmonic coefficients.

After this step, we created the bipartite graphs, where the source s is linked with each harmonic coefficient h_i of the query side , and the edges contain the harmonic coefficient value c_i.

To create the intermediary edges, after several tests with controlled 3D objects, we identified that, the maximum value between the harmonic coefficient c of the 3D medical object given as query Q_c and the consulted C_c resulted in the best differentiation, when two 3D medical objects are compared. In Figure 3 this step is represented by the Equation $max(Q_c, C_c)$.

Finally, following the same strategy of the source node, each edge of C side is connected to the sink node t with its respective harmonic coefficient c_i.

With the network flow created we can execute the Ford-Fulkerson method to obtain the residual flow of this bipartite graph.

V. Methodology

Given the background presented in the previous sections, we implemented SPHARMs and Ford-Fulkerson algorithms in order to apply them to 3D medical objects retrieval. Then, we designed a methodology to evaluate this approach to differentiate 3D medical objects with shape alterations. As a case study, we investigated the CHF disease, which causes small deformations in the left ventricle structure.

Our approach uses CBIR concepts to retrieve in a query those objects that are more similar to an object provided as argument. Thus, if an object of a patient with CHF is given as argument, the approach should retrieve objects of other patients with this disease; and vice-versa.

To retrieve the information we extracted the SPHARMs coefficients from the 3D left ventricles surface and compare them based on the residual flow information. To get the residual flow information we modeled the coefficients as a network flow problem, using bipartite graphs and applied the Ford-Fulkerson algorithm.

We evaluated the results using well-known information retrieval metrics and the processing time to execute the retrieval, as detailed following. The SPHARMs performance was compared with a global shape descriptor named 3D Hough Transform, which returned good results using the same dataset [22].

A. Hardware and Software Setup

The implementation tests and validation of our approach were executed in a computer with processor Intel i5, with 8GB of RAM and using Windows 7 OS - 64bits.

The algorithm was developed using Java JDK 1.8 in the Eclipse Helius IDE [23]. The Seg3D software [24] was used to manually segment the slices, and ImageVis 3D software [25] was used in the reconstruction process. For validation we used the *R* library [26] to process the results.

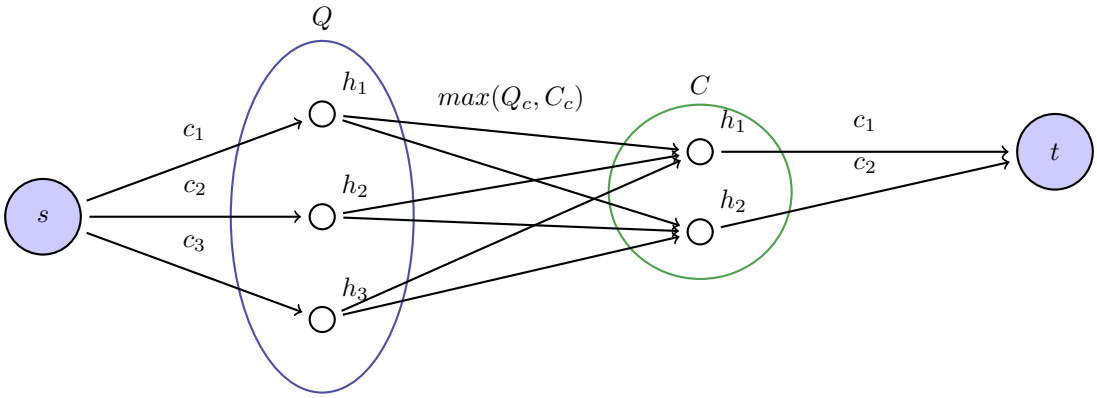

Figure 3. Example of a query in our our approach using SPHARMs and the network flow with bipartite graphs approach.

B. 3D medical objects

To validate our approach, we used 30 slices sets from cardiac MRI images. The sets were submitted to segmentation and reconstruction processes in order to obtain 3D medical objects of the left ventricle. From these cases, 47% are related to subjects without the CHF disease and 53% are subjects that have the disease. These cases are from 30 different patients with different ages and gender. To reconstruct the 3D objects, we selected the slices from short axis in a diastolic phase (when the left ventricle gets its maximum aperture). These slices have a resolution of 256x256 pixels and an slice offset average of 320 mm. At the end of the process we obtained about 10 slices per patient. This step was supported and validated by the research group of physicians from Heart Institute (Instituto do Coração - InCor), who approved the results.

We manually segmented the 2D MRI images by using open source software [24]. Figure 4a shows an example of a segmented slice and Figure 4b shows an example of a slices subset.

After segmentation, the contours of the ventricles segmented in all the slices of each set were joined to form a 3D object (a surface), also using open source software [25]. Figure 4c shows an example of left ventricle reconstructed after segmentation. Each reconstructed mesh has about 11000 vertices.

C. Evaluation

To evaluate the proposed approach to retrieve similar 3D objects we used different metrics: dendograms with hierarchical clustering to visualize how the groups' hierarchy was built, silhouette to validate the cluster separation, and Precision *vs.* Recall curve to compare the retrieval precision for each subset of cases (CHF and non-CHF subjects). We performed the retrieval one against all, considering all the 3D objects of the dataset. Then we computed the metrics from these results.

As mentioned, in Section V dendograms show how much the objects are similar through the hierarchical visualization, where the similar objects are grouped in branches. Thus, all the objects that belong to a branch are considered similar.

Silhouette coefficient is a well known metric to analyze the cluster division. This coefficient is defined in the interval $[0, 1]$, where higher values indicate strong division in the cluster, with well-divided groups; otherwise, lower values indicate the opposite [27]. Equations 9 and 10 present the silhouette coefficient computation (Sil_i). Considering an object o_i, a is the cluster that contains o_i, b is the set of all the other clusters that not contains o_i, and db_i is the minimum of the all average distances ($d_a(b)$) between o_i and the elements of each cluster of the b set. In our experiment we created two clusters: one for CHF group and other for non-CHF group.

$$db_i = min(d_a(b)) \tag{9}$$

$$Sil_i = (db_i - da_i)/max(a_i, db_i) \tag{10}$$

Precision *vs.* Recall curve is a traditional metric used for information retrieval problems [6]. The precision metric indicates the percentage of relevant objects retrieved in relation to the total of objects retrieved. The recall indicates the percentage of objects retrieved that are relevant in relation to the total of relevant objects present in the database. The larger the area between the curve generated and the x axis, the greater is the system accuracy. The values in both axis are in the normalized range [0,1] or can be expressed in percentage.

Equation 11 and Equation 12 present, respectively, the computation of precision and recall terms. The variable TP indicates true positive results, FP false positives and FN false negatives results. Considering our dataset, TP indicates relevant 3D objects retrieved, i.e., the 3D objects retrieved that belong to the same class (non-CHF or CHF) of the query. FP indicates 3D objects that are retrieved but do not belong to the class of the query. Finally, FN are 3D objects that are not retrieved but they belong to the query class.

$$Precision = TP/(TP + FP) \tag{11}$$

$$Recall = TP/(TP + FN) \tag{12}$$

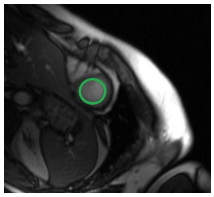

(a) MRI slice with the left ventricle segmented (green line).

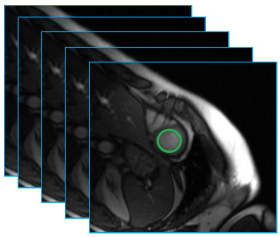

(b) Set of slices segmented

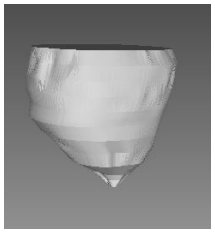

(c) Left ventricle reconstructed from MRI slices.

Figure 4. 3D medical objects creation steps.

VI. Results and Discussion

In this section the results obtained with the proposed approach are reported, comparing them with an approach that uses 3D Hough Transform and distance functions to retrieve the objects described in Section V. We chose the 3D Hough Transform because this method reported good results using the same dataset [28].

Figures 5a and 5b show the results by using Dendograms. It is possible to note that both approaches have good results. Most cases were retrieved in the correct class, but we saw less wrong cases retrieved (circled in red color in both Figures) when we applied the SPHARMs.

The wrong cases retrieved by 3D Hough Transform descriptor contain very subtle changes which were not correctly differentiated. 3D Hough Transform descriptor compares the 3D objects based on the amount of vertices that has similar spherical coordinates within an interval of distances from 3D object centroid and its surface. This grouping was defined in intervals of 90 degrees in our tests, and this parameter can limit the descriptor performance, since this grouping can lose information. Another point is related to Euclidean distance that compares each grouping as it is very sensitive to outliers stored in the feature vector, maybe producing wrong retrievals.

In the proposed approach, we obtained a more detailed description of the shape from each 3D object by using SPHARMS. Since all the coefficients are processed on the bipartite graph, few information is lost. Additionally, as mentioned in Section IV and Section V, the differences are highlighted when using the maximum value as the intermediary nodes, providing more accurate results.

Figure 6 shows the Precision *vs.* Recall curve of each approach in both scenarios (with and without CHF). Ratifying the dendograms behavior, we observed a better performance using the SPHARMs residual flow information. Our approach resulted in an average precision of 91.5% for CHF cases (the curve of Figure 6 denominated CHF-SPHARMs) and 89.6% for non-CHF cases (the curve of Figure 6 denominated non-CHF -SPHARMs), outperforming the 3D Hough Transform that reported an average precision of 85.8% for CHF cases and 79.8% for non-CHF cases. The improvement is more evident when the recall values in x-axis increases, this area is associated with the last 3D objects retrieved that has small differences compared to the 3D object given as query.

In practical terms, this indicates that our approach were more precise when the intention is to detect subtle differences among shapes, and capture more shape details when compared to the 3D Hough approach. This corroborates our affirmative that the improvement caused by our approach is derived from the SPHARMs capability to extract from 3D objects very detailed information about their structure, as well as from our strategy to modeling the coefficient comparison as a network flow problem in order to use the residual flow as similarity measure.

Regarding to the silhouette value, we found a value of 0.68 for 3D Hough Transform descriptor. Using SPHARMs and network flows we increased this value to 0.73, an improvement of 7%, indicating that SPHARMs are more discriminative and the clusters are more correctly separated.

Finally, related to time to process the 3D Hough Transform descriptor takes, in average, 4 seconds to execute the extraction and compute the similarity for each query given. In our novel approach the whole process takes, in average, 1.4 seconds, causing an improvement of 65%. For real time applications, this difference is significant. Nowadays, the user experience (UX) requires a system without significant delay in any industry segment. Especially for health care, beyond the UX expectation, we are dealing with patient expectation: faster diagnosis can favor early detection of possible diseases, and, consequently, contribute to start therapies earlier. Finally, if we can provide faster diagnosis, this can imply in cost reduction in health care chain.

We verified that the additional process to displace the coefficients in order to create the intermediary edges' values, did not influence negatively the processing time in the retrieval task. To find the most negative number, the computational complexity verified is O(1), and besides the sum needs to be executed in all other harmonic coefficients, with a computational complexity O(n), it takes 2 milliseconds to be completed.

In addition to the better results confirmed with the three metrics above, the proposed approach outperforms classical shape descriptors in other aspects, as described following.

Regarding SPHARMs, we noted a greater flexibility to use

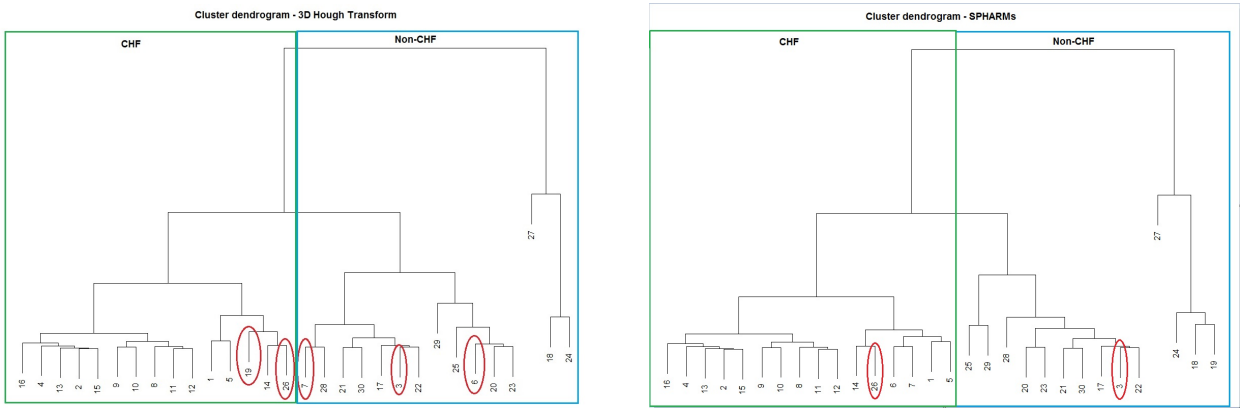

(a) 3D Hough Transform and Euclidean Distance

(b) SPHARM and Ford-Fulkerson

Figure 5. Results of the groups using a Dendogram: the green box is related to CHF cases and blue box are subjects without the disease.

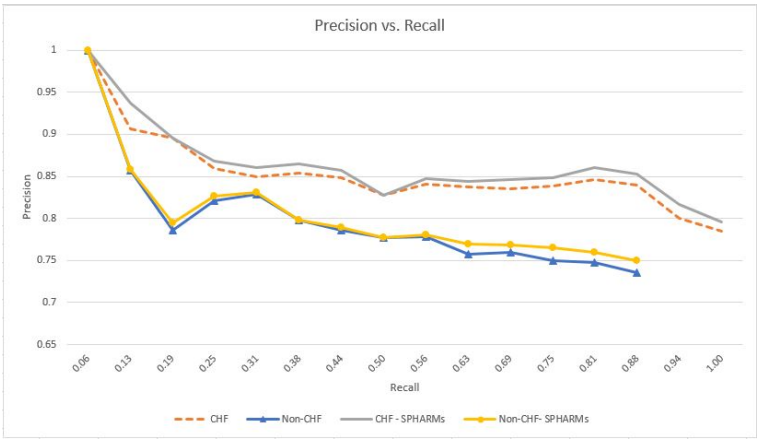

Figure 6. Precision *vs.* recall curve for CHF and non-CHF cases and comparing the two approaches.

their coefficients as local descriptors. In this evaluation, we compared the whole left ventricle, but it is possible to the expert select a specific area of the 3D left ventricle to be analyzed. Since the SPHARMs use the spherical coordinates of each vertex, we can build the bipartite graph just with the points selected by them. In other approaches we cannot perform that in a transparent way as SPHARMs. Usually researchers develop descriptor specifically for local purposes for 3D context; we noted a predominance of view-based descriptors, which process and compare different "views" of the 3D object, and bag-of-words descriptors that use semantic strategy to label specific parts of the 3D objects [3]. In [29] the left ventricle is investigated using SPHARMs as a rotation invariant descriptor, in this work, 33 cases separated between healthy and with myocardial disease patients were analyzed. The authors reported a mean precision of 50% and discussed that in despite of they investigated the left ventricle shape in 17 different regions, maybe better results can be obtained by sorting the left ventricle in more regions. In our approach it is not necessary split the left ventricle to obtain the local shape information, improving the data quality.

Another advantage of our approach is associated to network flows, that can be used as similarity comparison method. In L_p distances, the metric most used on CBIR problems, we must have the feature vector with the same size to avoid discrepant values. Thus, it is necessary to elaborate the method to extract features taking in account how store the information in the feature vector. 3D Hough Transform, for example, uses the grouping strategy to ensure the same feature vector size [28]. In SPHARMs, which generates one coefficient per vertex, it is almost impossible to ensure that all the reconstructed objects will have the same amount of vertices. Thus, or we adapt the manner as the feature vector is built or we select the amount of points that will be processed by SPHARMs – in both approaches we are assuming the risk to loose information. Using the network flow we did not face this type of problem. It is possible to compare different amount of SPHARMs coefficients, since the network flow was modeled using a complete bipartite graph, that is, each coefficient of a Q class is connected to the all other coefficients of class C class, and the residual flow represent the difference between these classes.

We tested our approach with 30 cases that were properly classified by experts. Tests with more cases that have dif-

ferent shape characteristics are welcome. Due that, we are planning to extend the tests in a more generic context, of Cardiomyopathies. In addition, from the results obtained, we can assume that 3D objects with similar characteristics (convex and with subtle changes in the shape) can take advantage of the proposed approach, obtaining good precision in retrieval problems.

VII. Conclusion

In this paper, we propose a novel approach to retrieve 3D medical objects of left ventricle reconstructed using the SPHARMs and network flows concept. The main innovation achieved by our research comes from the utilization of network flows as similarity measure, due to the useful information returned on residual flows.

We obtained an average precision of 85.8% for CHF cases and 79.8% in a previous approach, which is a positive result for this kind of application. Our novel approach detailed in this article, however, outperformed those values in about 10% and for CHF cases we got an average precision of 91.5% and for non-CHF cases 89.6%. Additionally, our approach is more flexible, since it allows different feature vector sizes and we can both analyze the 3D object globally or locally, a desirable characteristic in the medical image processing problems. Finally, with those results we will test our approach in a expanded scenario with a generic cardiac disease, denominated Cardiomiopaty.

Acknowledgment

This work is supported by Brazilian National Council of Scientific and Technological Development, the - Brazilian Federal Agency for Support and Evaluation of Graduate Education (CAPES), Sao Paulo Research Foundation (FAPESP) and the National Institute of Science and Technology Medicine Assisted by Scientific Computing.

References

[1] Standford, "Stanford Medicine 2017 Health Trends Report," Tech. Rep., 2017.

[2] R. Datta, D. Joshi, J. Li, and J. Z. Wang., "Image retrieval: Ideas, influences, and trends of the new age," ACM Comput. Surv., vol. 40, no. 2, pp. 5:1–5:60, 2008.

[3] F. Yu, Z. Lu, H. Luo, and P. Wang, Three-dimensional model analysis and processing. Springer Science & Business Media, 2011.

[4] M. Kazhdan, P. Simari, T. McNutt, B. Wu, R. Jacques, M. Chuang, and R. Taylor, "A shape relationship descriptor for radiation therapy planning." Medical image computing and computer-assisted intervention : MICCAI ... International Conference on Medical Image Computing and Computer-Assisted Intervention, vol. 12, no. Pt 2, pp. 100–8, 2009. [Online]. Available: http://www.ncbi.nlm.nih.gov/pubmed/20426101

[5] F. H. Martini and F. Martini, Fundamentals of anatomy and physiology. Prentice Hall, 1992.

[6] H. Muller, N. Michoux, D. Bandon, and A. Geissbuhler, "A review of content-based image retrieval systems in medical applications—clinical benefits and future directions," International journal of medical informatics, vol. 73, no. 1, pp. 1–23, 2004.

[7] A. W. M. Smeulders, M. Worring, S. Santini, A. Gupta, and R. Jain, "Content-based image retrieval at the end of the early years," Pattern Analysis and Machine Intelligence, IEEE Transactions on, vol. 22, no. 12, pp. 1349–1380, 2000.

[8] T. H. Cormen, C. Stein, R. L. Rivest, and C. E. Leiserson, Introduction to Algorithms, 2nd ed. McGraw-Hill Higher Education, 2001.

[9] G. B. Arfken and H. J. Weber, Mathematical methods for physicists, 7th ed. Elsevier, 1992.

[10] H. Groemer, Geometric applications of Fourier series and spherical harmonics. Cambridge University Press, 1996, vol. 61.

[11] R. Diestel, Graph theory. Springer Publishing Company, Incorporated, 2017.

[12] W. B. H. Khelifa, A. Ben Abdallah, and F. Ghorbel, "Three dimensional modeling of the left ventricle of the heart using spherical harmonic analysis," in Biomedical Imaging: From Nano to Macro, 2008. ISBI 2008. 5th IEEE International Symposium on, 2008, pp. 1275–1278.

[13] M. E. Shenton, G. Gerig, R. W. McCarley, G. Székely, and R. Kikinis, "Amygdala–hippocampal shape differences in schizophrenia: the application of 3D shape models to volumetric {MR} data," Psychiatry Research: Neuroimaging, vol. 115, no. 1–2, pp. 15–35, 2002. [Online]. Available: http://www.sciencedirect.com/science/article/pii/S0925492702000252

[14] N. Cao, X. Liang, Q. Zhuang, and J. Zhang, "Approximating high angular resolution apparent diffusion coefficient profiles using spherical harmonics under BiGaussian assumption," in SPIE Medical Imaging, vol. 7262, 2009, pp. 726 204–726 208.

[15] X. Chen, W. Li, J. Hua, X. Zhang, and H. He, "Shape manifold regression with spherical harmonics for hippocampus shape analysis," in SPIE Medical Imaging, vol. 8669, 2013, pp. 866 940–866 949.

[16] G. Coppini, M. Demi, P. Marraccini, and A. L'Abbate, "3-D heart motion from X-ray angiography," in Computers in Cardiology 1995, 1995, pp. 71–74.

[17] S. Eck, S. Wörz, K. Müller-Ott, M. Hahn, G. Schotta, K. Rippe, and K. Rohr, "3D shape analysis of heterochromatin foci based on a 3D spherical harmonics intensity model," in SPIE Medical Imaging, vol. 9034, 2014, pp. 90 340X–90 340X–6.

[18] H. Edvardson and O. Smedby, "Compact and efficient 3D shape description through radial function approximation," Comput Methods Programs Biomed, vol. 72, no. 2, pp. 89–97, 2003.

[19] M. Styner, G. Gerig, J. Lieberman, D. Jones, and D. Weinberger, "Statistical shape analysis of neuroanatomical structures based on medial models," Medical Image Analysis, vol. 7, no. 3, pp. 207–220, 2003.

[20] M. Styner, J. A. Lieberman, D. Pantazis, and G. Gerig, "Boundary and medial shape analysis of the hippocampus in schizophrenia," Medical Image Analysis, vol. 8, no. 3, pp. 197–203, 2004.

[21] M. Kazhdan, T. Funkhouser, and S. Rusinkiewicz, "Rotation invariant spherical harmonic representation of 3D shape descriptors," in Proceedings of the 1th Eurographics/ACM SIGGRAPH symposium on Geometry processing, no. 1. Aachen, Germany: Eurographics Association, 2003, pp. 156–164.

[22] L. C. C. Bergamasco and F. L. S. Nunes, "Three-dimensional Content-Based Cardiac Image Retrieval using global and local descriptors," in AMIA Annual Symposium Proceedings. Washinghton, USA: AMIA, 2015, pp. 1811–1820.

[23] Eclipse, "Eclipse IDE," 2017. [Online]. Available: www.eclipse.org

[24] CBIC, "Seg3D: Volumetric Image Segmentation and Visualization. Scientific Computing and Imaging Institute (SCI)," www.sci.utah.edu/cibc-software/seg3d.html, 2012.

[25] ——, "ImageVis3d: A Real-time Volume Rendering Tool for Large Data. Scientific Computing and Imaging Institute (SCI)," www.sci.utah.edu/software/imagevis3d.html, 2012.

[26] R. Programming, "R Programming," 2017. [Online]. Available: https://www.r-project.org

[27] P. J. Rousseeuw, "Silhouettes: A graphical aid to the interpretation and validation of cluster analysis," Journal of Computational and Applied Mathematics, vol. 20, pp. 53–65, 11 1987.

[28] L. C. C. Bergamasco and F. L. S. Nunes, "A New Local Feature Extraction Approach for Content-based 3D Medical Model Retrieval Using Shape Descriptor," in Proceedings of the 29th Annual ACM Symposium on Applied Computing, ser. SAC '14. New York, NY, USA: ACM, 2014, pp. 902–907. [Online]. Available: http://doi.acm.org/10.1145/2554850.2554873

[29] R. Ayari, A. B. Abdallah, R. Sfar, F. Ghorbel, and M. H. Bedoui, "Analysis of regional deformation of the heart's left ventricle using invariant {SPHARM} descriptors," {IRBM}, vol. 35, no. 5, pp. 226–232, 2014. [Online]. Available: http://www.sciencedirect.com/science/article/pii/S1959031814000773